This is a peer-reviewed, accepted author manuscript of the following research article: Arnaoutakis, GE, Busko, D, Richards, BS, Ivaturi, A, Gordon, JM & Katz, EA 2024, 'Ultra-broadband near-infrared upconversion for solar energy harvesting', *Solar Energy Materials and Solar Cells*, vol. 269, 112783. https://doi.org/10.1016/j.solmat.2024.112783

Ultra-broadband near-infrared upconversion for solar energy harvesting

Georgios E. Arnaoutakis [1,2,*], Dmitry Busko [3], Bryce S. Richards [3,#], Aruna Ivaturi [4], Jeffrey M. Gordon [1], Eugene A. Katz [1]

[1]*Department of Solar Energy and Environmental Physics, Jacob Blaustein Institutes for Desert Research, Ben-Gurion University of the Negev, Sede Boqer Campus, 8499000, Israel*

[2]*Department of Mechanical Engineering, School of Engineering, Hellenic Mediterranean University, Heraklion, Greece*

[3]*Institute of Microstructure Technology, Karlsruhe Institute of Technology, Hermann-von-Helmholtz-Platz 1, 76344 Eggenstein-Leopoldshafen, Germany*

[4]*Smart Materials Research and Device Technology Group, Department of Pure and Applied Chemistry, University of Strathclyde, Glasgow, G1 1XL, UK*

*Corresponding authors, e-mail: * arnaoutakis@hmu.gr , # bryce.richards@kit.edu*

Abstract

Upconversion – the absorption of two or more photons resulting in radiative emission at a higher energy than the excitation – has the potential to enhance the efficiency of solar energy harvesting technologies, most notably photovoltaics. However, the required ultra-high light intensities and the narrow absorption bands of lanthanide ions limit efficient solar utilisation. In this paper, we report results from exciting upconverters with concentrated sunlight at flux densities up to 2300 suns, where the radiation is restricted to photon energies below the bandgap of silicon (corresponding to a wavelength $\lambda = 1200$ nm). Upconversion to $\lambda = 980$ nm is achieved by using hexagonal erbium-doped sodium yttrium fluoride (β-$NaYF_4$: Er^{3+}) in a fluoropolymer matrix. Upconversion has a nonlinear relation with irradiance, therefore at a high irradiance a threshold occurs where the process becomes linear. For β-$NaYF_4$:25%Er^{3+}, we find a two-photon threshold under concentrated sunlight at 320 suns. Notably, this threshold is lower than under corresponding laser excitation and can be related to all resonantly excited Er^{3+} ion levels and excited stated absorption. These results highlight a pathway that utilises a far broader portion of the solar spectrum for photovoltaics.

Introduction

Up-conversion (UC) is a non-linear photonic process whereby the energy from two or more lower energy photons can be added to result in the emission of a single higher energy photon [1]. UC has been investigated for applications in lasers [2], biomedical imaging [3], [4], anti-counterfeiting [5], [6], plastic recycling [7] and solar energy harvesting [8], [9], [10]. For photovoltaics, it can be a promising method for circumventing solar cell transmission losses associated with sub-bandgap photons in the solar spectrum [11]. Calculations show that UC could increase the theoretical upper efficiency (Shockley-Queisser) limit of single-junction solar cells from 33% to 48% [11], in the ideal case. Efficient rare-earth [12], [13], [14] upconverters have been reported with up to 9.5% external UC quantum yield (eUCQY), which is the ratio of externally emitted to incident photons. Rare earth upconverters with high near-infrared (NIR) eUCQY were found to exhibit the highest performance for silicon [14], [15] and perovskite solar cells [16].

In trivalent lanthanide ions, UC occurs via radiative transitions within the partially filled *4f* shell. The first excited state is populated via ground state absorption (GSA). Excited-state absorption (ESA) of an additional photon can produce a higher excited state. However, a more efficient process – especially at lower excitation power densities – can occur *via* energy transfer upconversion (ETU) to the nearby activator ions at the first excited state, as depicted in **Fig. 1(a)**. The energy of one ion is donated to a nearby ion, promoting it to a higher metastable state, while the energy of the sensitizer returns to the ground state.

In a simplified three-level system where the rate of ETU to the first excited state, W_1, is the dominant mechanism and ESA is neglected, the population density N_1 of the first excited state will depend on the rate R of multi-phonon relaxation and linear decay as [17], [18]:

$$W_0 N_0 N_S = (R + W_1 N_S) N_i , \qquad (1)$$

where W_0 is the rate of the ETU to the ground state transition and N_S the population density of the sensitizer. Because the population depends on the absorption cross section of the sensitizer, it is irradiance E (in W/m^2) rather than power P (in W) that serves better for comparisons between different experiments, independent of the excitation beam size and spectral bandwidth.

At a low irradiance E, where depopulation to the ground state is dominant, $R >> W_1 N_S$ and the relation becomes [18]:

$$N_S \propto \sigma E^n , \qquad (2)$$

where σ is the absorption cross section of the sensitizer and n is the integer number of photons involved in the UC process. The value of n is commonly obtained from log-log plots of the integrated UC photoluminescence (UCPL) versus E (**Fig. 5**). For the two-photon threshold investigated here at low power, we deduce $n = 2$. At high P, the emission to the ground state will be minimal and UC to the higher energy state is the main depopulation mechanism, for which $W_1 N_1 N_S >> R N_1$, and $n = 1$, thus Eqn. (2) becomes [18]:

$$N_S \propto \sigma E . \qquad (3)$$

The maxima of the absorption lines of each state may be at different wavelengths. As a consequence, the maximum absorption cross section of each excited state may require a different photon energy for maximum population. In this case, monochromatic laser excitation may not provide the required photon energy, while lasers of different wavelengths or broadband excitation sources are suitable to optimize the efficiency of each step involved in upconversion [19].

The irradiance required to populate the excited states can, moreover, be quite different for laser vs. solar excitation. For solar energy applications, the irradiance is a function of the non-dimensional absorbance-weighted solar concentration C_A defined as the ratio of the integrals of the absorbance-weighted spectral excitation irradiance $E_{exc}(\lambda)$ between the source and the air-mass 1.5 direct (AM1.5D) solar spectrum [20], [21], [22]:

$$C_A = \frac{\int A(\lambda) E_{exc}(\lambda) d\lambda}{\int A(\lambda) E_{AM1.5}(\lambda) d\lambda}, \qquad (4)$$

where $A(\lambda)$ denotes spectral absorbance, and the integrations in Eqn. (4) cover the entire solar spectrum (λ = 280-4000 nm). Solar concentration is expressed here in the units of "suns" (*i.e.*, the ratio of target irradiance relative to the incident solar beam irradiance) is independent of the spectrum, and hence considerably greater than C_A.

There have been considerable efforts towards engineering upconverters for the practical regime of low-irradiance thresholds [23]. For two-photon UC, a straightforward method to estimate this threshold is to observe the irradiance where the slope of the log-log plot of UCPL against E reaches 1.5 [24]. UC laser thresholds as low as 10 W/m^2 were reported in surface-anchored metal-organic-framework heterojunctions [25] – achieved by creating controlled phase-separated structures in the heterojunctions, and offering additional routes for low-threshold or even threshold-less UC [26]. In a similar organic-inorganic route, efficient dye-sensitised UC was demonstrated [27] in a system of $NaYGdF_4:Yb^{3+}Er^{3+}$ sensitised by a carboxylated dye at very high thresholds of 1.8×10^4 W/m^2. The sensitization of Er^{3+} ions to extend its infrared response has been demonstrated with Ni^{2+} ions [28] within the band λ = 1060-1450 nm, and with size-engineered PbS quantum dots over λ = 1100-1470 nm [29] bridging the gap between the absorption of crystalline silicon (c-Si) and Er^{3+} ions, as well as the directional emission by arrays of photonic-crystals [30]. Christiansen *et al.* [31] reported an analytical model for the intensity dependence of UC in Er^{3+} ions from excitation at λ = 1500 nm to emission at λ = 980 nm.

They observed a saturation at 5×10^3 W/m^2 for $NaYF_4$: Er^{3+} nanoparticles, with similar irradiance values recently reported [32] for the NIR-to-visible (980 nm to 550 nm) UC of $NaYF_4$: 18%Yb^{3+}, 2%Er^{3+} microcrystals. At the saturation irradiance, UC is the dominant depopulation process and the eUCQY no longer depends on excitation power. It was found [32] that at the saturation eUCQY is 5.8 greater than the PLQY of the specific energy level at the irradiance of the threshold.
The irradiance thresholds under a broadband solar excitation must be far higher than with laser excitation, because i) the radiance of the sun is far below that of lasers, and ii) a large fraction of solar power is contained in spectral regions that do not yield any UC. Nonetheless, a broadband input can excite a wider range of photons at excited states, with the most probable state being $^4I_{13/2}$. Indeed, Fischer *et al.* reported on the eUCQY of β-$NaYF_4$: 25%Er^{3+} under different spectrally-broad bands [21]. The eUCQY of β-$NaYF_4$: 25%Er^{3+} saturates at a lower irradiance when the excitation is at λ = 1450-1600 nm compared to the excitation covering 1500-1550 nm. For a lower erbium content, β-$NaYF_4$: 10%Er^{3+} saturation was reported at 1490-1550 nm at an irradiance of 2.27×10^6 W/m^2 [33], [34]. Moreover, when compared to an oxysulphide host lattice, Gd_2O_2S: 10%Er^{3+}, there was a higher eUCQY under broadband excitation [35] due to a broader absorption of the solar spectrum, suggesting that the fluoride host is better suited for solar applications.

Because the clear-sky, mid-day solar irradiance on earth is approximately 1000 W/m^2, therefore a form of solar concentration is required to obtain sufficiently high irradiance on the upconverter. Solar concentration also improves the optical efficiency of the system. 1.7× stronger upconversion was reported with dielectric microbeads [36], and comparable improvements were found with commercial dielectric compound parabolic concentrators exhibited improvements with a concentration ratio of 2.8× [22] independent of the irradiance on the overlying solar cell. A 2.7× enhancement was reported by applying an upconverter-coated double-layered metasurface [37], while improvements of ~100× [8], [38], [39] and up to 3 orders of magnitude [40] were reported by utilizing dielectric microlens arrays. Although the reported concentrators increased the target irradiance, the upconverter may require several orders of magnitude higher concentration, which has shown to be possible [41]. Reaching such a high solar irradiance mandates accurate dual-axis solar tracking, for which dual reflector optics have been found to provide a liberal optical tolerance to off-axis orientation [42].
In this paper, we utilized the reflective-refractive solar concentrators shown in **Fig. 1(b)**. A two stage solar concentrator that covers the irradiance values involved in the transition from the two-photon to the linear regime was utilized. Previous upconverter devices required that the upconverter be directly attached to the back of the solar cell, which limited the available concentration to a few hundred suns, as a higher concentration would diminish the efficiency of the solar cells due to Auger recombination. As seen in **Figure 1(b)**, the proposed configuration enables very high concentrations levels at the upconverter, while the overlying silicon solar cell enjoys a low concentration of 15 suns. This configuration offers the advantage of realizing maximum solar cell efficiency, while ensuring the high solar concentrations levels needed to excite the upconverter. A major advantage of physically separating the solar cell and the upconverter (**Fig. 1(b)** is the collection of the diffuse sunlight at the back side of the bifacial solar cell. Concurrently, high concentration is achieved by a secondary concentrator that collects the UC luminesced to the underside of a bifacial cell. Only a fraction $1/C$ of the diffuse radiation is collectible, where C denotes the geometric concentration which, at the flux densities required for UC, this means that essentially no diffuse light reaches the upconverter.
In addition, extended excitation bandwidths are investigated in β-$NaYF_4$: Er^{3+} embedded in a commercially available fluoropolymer matrix, which exhibits one of the highest eUCQY in the infrared [15]. Drawing from the experience of UC in silicon photovoltaics and aiming to examine broader bandwidths that may provide photons for additional transitions, we utilise most of the sunlight transmitted through silicon ($\lambda > 1100$ nm), at a solar flux concentration values up to 2300 suns. These are flux densities that are tractable with commercial optical systems.

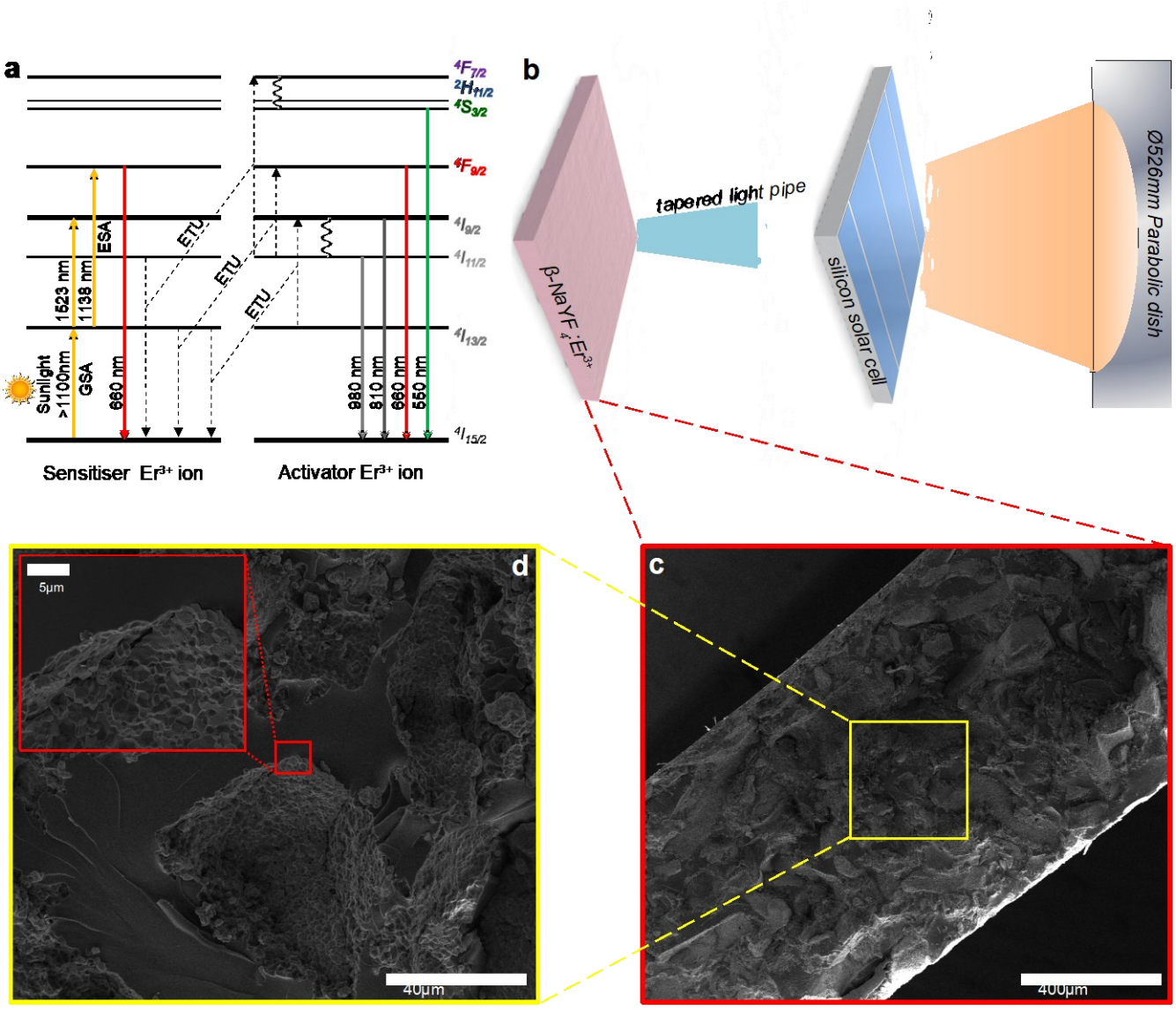

Figure 1: Photovoltaic Upconversion where at least two sub-bandgap solar photons at $\lambda > 1100$ nm (for silicon) are converted into one photon above the bandgap energy. a) Energy level diagram of the Er^{3+} ion system, showing the transitions involved in two- and three-photon UC under concentrated sunlight at $\lambda > 1100$ nm. b) The parabolic and tapered concentrators are needed to irradiate with flux densities of 15 suns on silicon and 2300 suns on the upconverter. c) SEM cross-section of the upconverter β-$NaYF_4$:Er^{3+} embedded in perfluorocyclobutyl (PFCB) matrix with 55.6% w/w ratio, d) Magnification of the SEM displaying spatially separated regions of upconverter and PFCB. Smaller than 5 µm porous grains of the upconverter can be seen in the inset.

Methods & Materials

The UC consisted of a β-$NaYF_4$ micro-crystalline phosphor, doped with 5, 15, 25, 35, 50 and 75% Er^{3+} ions. The samples were synthesized at the University of Bern following the recipe described in [43]. The phosphor was cast in a perfluorocyclobutyl (PFCB) polymer (Tetramer Technologies LLC, USA) matrix, at a phosphor-to-polymer weight ratio of 55.6% according to the methods in references [12] and then finally cut and polished into 1 mm-thick discs of 12.5 mm diameter. PFCB was chosen for its low absorption coefficient in the NIR, as well its refractive index closely matching that of the β-$NaYF_4$: Er^{3+}. The size of the β-$NaYF_4$ crystal, see **Fig. 1(c,d)**, resulted in inhomogeneous scattering, which may affect the collection efficiency of the emission at oblique angles. Clusters of β-$NaYF_4$ crystals up to 50 µm can be seen, encapsulated by the PFCB polymer. The porous β-$NaYF_4$ clusters are

large compared to their encapsulation in polydimethylpolysiloxane (PDMS) [37] in addition to limited water and oxygen penetration [44]. This work focused on one of the most efficient upconverters, which was encapsulated in a stable solid state matrix to enable the presented characterization. Considering the stability of the fluoropolymer matrix, future research can consider incorporating core-shell nanoparticles into an equivalent matrix [45].

Direct sunlight was concentrated with two optical systems previously described in detail [46], [47]. In the first system (**Fig. 2a**), a parabolic mini-dish, 20 cm in diameter (mounted on a dual-axis solar tracker), with a secondary flat mirror that re-images the solar disc into an optical fibre with a fused-silica core diameter of 1.00 mm and a nominal numerical aperture *NA* of 0.66, delivered target irradiance values of 27-235 suns onto the upconverter at a distance $L = 2$ mm below the fibre tip. The excitation beam width w was measured with the knife-edge technique (**Fig. S1**), and calculated as $w = 2\times\tan(\mathrm{ArcSin}(NA))+L$, yielding an illumination area of 0.16 ± 0.02 cm^2. The beam profile at the end of the fibre is not uniform [48], so different irradiance values may produce different UCQY [49] - a point for future investigation. UCPL was detected from the edge of the sample by an optical fibre with a core diameter of 0.60 mm.

The second concentrator (**Fig. 2b**) is a solar furnace comprising an outdoor flat mirror that tracks the sun and reflects the beam to a stationary indoor parabolic dish, 52.6 cm in diameter, with $NA = 0.40$. A truncated square pyramidal light pipe made of BK7 glass (Edmund Optics, 63105) that served as a flux-homogenising rod was inserted with its larger aperture at the focus of the dish, delivering a uniform spatial distribution over an exit area of 16 ± 0.09 mm^2 on the upconverter. The tapered light pipe was selected due to its precision, while parabolic concentrators are usually the practical high-flux solar concentrator of choice [50] for their superior concentrating and collecting properties. The range of solar concentration attained with this configuration was 116-2300 suns. The UCPL was collected through the same light pipe by a 100 x 100 mm Fresnel lens, focusing to an optical fibre-coupled spectrometer (Stellarnet, BLK-C-SR). Sunlight at $\lambda < 1200$ nm was filtered by double-sided polished p-type float zone Si(100) wafers without any additional coatings. A longwave-pass filter (Thorlabs, FEL1350) was used to exclude photons absorbed by excited states. In both configurations, the UCPL from the surface of the sample at variable solar concentration (**Fig. S2**) was detected with minimal reabsorption, as in prior fluorescence measurements [51], [52]. The difference in the collection efficiency of the two optical systems resulted in different integrated UCPL intensities. Consequently, as a consistency check, we confirmed that the slopes of the power-dependent UCPL at irradiance values common to both concentrators were equal.

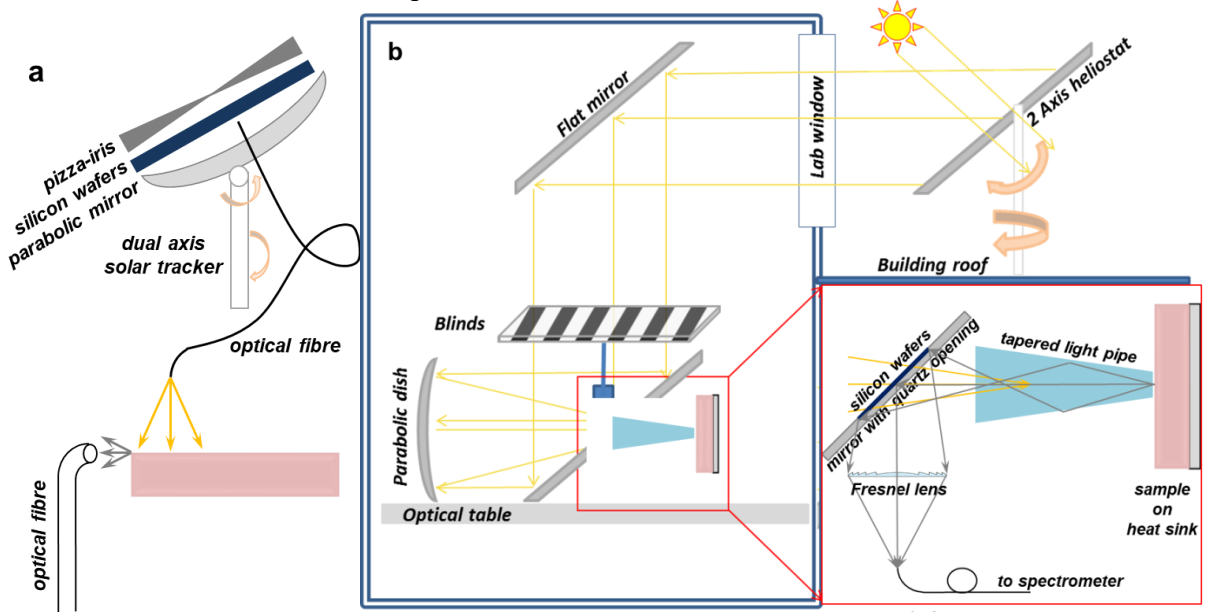

Figure 2: Schematics of the two different solar concentrator systems used in the study: a) parabolic mini-dish concentrator with optical fibre output, and b) solar furnace that includes a glass homogenising rod for uniform target illumination. In both configurations, sunlight at $\lambda < 1200$ nm was filtered out by silicon wafers.

The samples were mounted on a 75 x 60 x 50 mm aluminium heat sink. The upconverter temperature, monitored by thermocouples, was kept constant at 32±2ºC. The same temperature was also maintained when the delivered concentrated sunlight was passed through an optical chopper wheel (which preserves the instantaneous irradiance but can markedly lessen the time-averaged irradiance and hence the thermal load) as described in [53]. This resulted in the same excitation-dependent slopes, as also confirmed by the time-dependent kinetics of the UCPL spectra (**Fig. S3**). In the first 80 s of illumination at 1680 suns, the peaks at 550 nm, 660 nm, 810 nm and 980 nm remained constant, indicating that the emission from these levels is not thermodynamically coupled to the excitation. This confirms that illumination-induced heating did not occur during the measurements, and means that thermal correction factors, such as those suggested in reference [54] are not required here. Because the heating of solar cells under concentrated sunlight may affect their stability, future investigations should consider a temperature-controlled characterization [55].

The direct normal irradiance (DNI), measured by a pyrheliometer, varied between 866 and 915 W/m^2 during the experiments, conducted at Midreshet Ben-Gurion, Israel, (Lat. 30.8ºN, Long. 34.8ºE, Alt. 475 m) between July 2018 and June 2019. The power on the sample was measured with a thermal (spectrum-neutral) power-meter (Ophir, FL250A) the sensor of which was placed flush against the exit of the optical fibre or homogenising rod. Two sets of measurements were conducted as a function of the solar concentration: one set under the full solar spectrum, and the other set filtered by silicon wafers, *i.e.*, delivering only radiation at $\lambda > 1100$ nm.

Benchmark and high resolution irradiance experiments with monochromatic illumination (**Fig. S2**) were conducted at the Karlsruher Institute for Technology (KIT). A NIR laser (Thorlabs, TLK-L1550R) was utilized with a bandwidth reported by the manufacturer as 0.001 pm at $\lambda = 1523$ nm. The integrated irradiance at $\lambda > 1100$ nm, weighted by the absorbance of Er^{3+} ions is 10 W m^{-2}. The power and the area of the laser were measured with an IR-sensitive sensor (Thorlabs, S122C) and a slit beam profiler (Thorlabs, BP209-IR/M), respectively. Reflectance spectra were measured in a UV-Vis-NIR spectrophotometer (Cary-Agilent, 5000) equipped with an integrating sphere (Cary, Internal DRA 2500) and absolute reflectance standards (Labshere, SRT-99-020). 1523 nm laser excitation with $\Delta\lambda = 40$ nm was provided by a super-continuum laser with an acousto-optical filter, as previously reported [33].

Results & Discussion

Fig. 3 shows UCPL spectra under sunlight excitation at $\lambda > 1100$ nm. UC emissions were observed from energy level $^4I_{11/2}$ at 980 nm, $^4I_{9/2}$ at 810 nm, $^4F_{9/2}$ at 660 nm, $^4S_{3/2}$ at 550 nm and a weak emission at 525 nm from level $^2H_{11/2}$, see energy level diagram of **Fig. 1(d)**. No other luminescence was detected with sunlight excitation at $\lambda > 1100$ nm, which is consistent with other works on Er^{3+} ion UC using highly doped β-$NaYF_4$ and indicating that ETU is dominant.

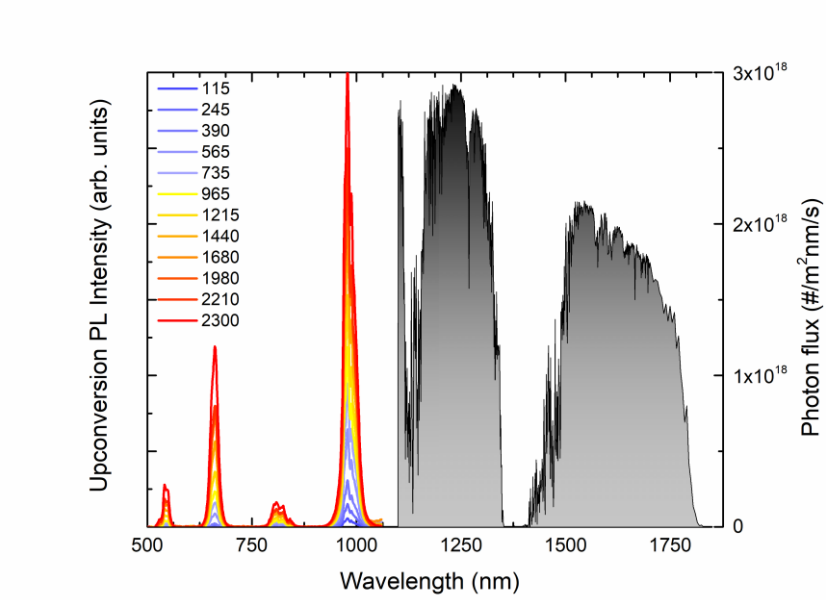

Figure 3: UCPL spectra of β-$NaYF_4$: 25%Er^{3+} for λ = 500-1100 nm under sunlight excitation at λ > 1100 nm (in grey) over solar concentration from 115 to 2300 suns available by the concentrators.

All spectral peaks were broadened compared to the 1523 nm laser excitation, shown in **Fig. 4**, suggesting cooperative processes between all resonantly excited energy levels come into play under a broadband excitation. This is in agreement with the homogeneous broadening of the external quantum efficiency (EQE) in upconverter solar cell devices, as reported under simultaneous laser and white-light bias [56]. The EQE of upconversion devices agrees with the excitation spectrum of the upconverter. In addition, the two-to-one photon emission at 980 nm, which is the most applicable emission for silicon solar cells, is the most intense. The integrated intensity of this emission will be used below to establish the solar concentration threshold for two-photon UC.

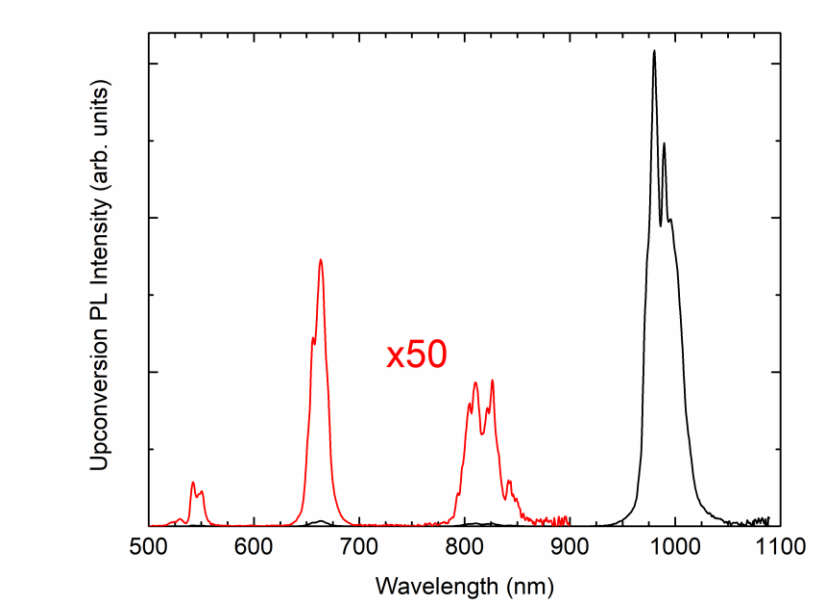

Figure 4: UC spectra of β-$NaYF_4$: 25%Er^{3+}, with the emission between 500 nm and 900 nm multiplied by 50x (red) relative to the excitation intensity (black).

Fig. 5 shows the power density dependence of the integrated UCPL at 980 nm under various excitation bandwidths are displayed. For a 1523 nm laser excitation (blue diamonds), the slopes of the UCPL curves were 1.91 at low irradiance and 1.17 at high irradiance. The slope of n=1.17 for laser excitation indicates that the two-photon process has not been reached, but is approaching saturation. The highest laser irradiance was approximately 7000 W/m^2 which, using Eqn. (4), corresponds to C_A = 410 suns.
When an excitation bandwidth at $\lambda > 1100$ nm is used (red circles), a slope of n=2.16 is obtained in the low-irradiance regime, consistent with two-photon UC ($n = 2$ in Eqn. (2)). A slope of n=1.57 is obtained at around 100 suns. This slope agrees well with the value of the balancing power density [24] where linear decay and ETU have equal contributions to the depopulation of the emitting state. A slope of 1.01 is obtained in the high-concentration regime, *i.e.* between 320-850 suns. The slope indicates that the $^4I_{11/2}$ level has a higher population, with a saturated two-photon solar UC. This is in agreement with the saturated eUCQY of β-NaYF$_4$: 25%Er^{3+} for a 1450-1600 nm excitation when compared to a lower excitation bandwidth of 1500-1550 nm [35], [57]. An eUCQY of 1.25% was reported for β-NaYF$_4$: 25%Er^{3+}, for an excitation of 1450-1600 nm [21], indicating the importance of high eUCQY for applications utilizing an incoherent excitation such as sunlight. The saturation of the two-photon process suggests depopulation of the emitting level through energy transfer by a higher-energy photon [20]. This is in agreement with the corresponding plots for the of the 660 nm integrated intensity, as will be shown below.
When the upconverter was excited by a laser with a 40 nm bandwidth (green triangles), two irradiance regimes could be seen. The slopes start from $n = 2$ at the lower irradiance and saturate to $n = 1.02$ at high irradiance. The solar concentration is noted at the top horizontal axis. The highest irradiance of 1.08x10^6 W/m^2 (delivered by the laser with a 40 nm bandwidth) saturated the upconverter. For the same irradiance, sunlight at $\lambda > 1100$ nm provides more photons than the laser. Saturation under sunlight was achieved at only 850 suns, while the onset of saturation began at 320 suns.

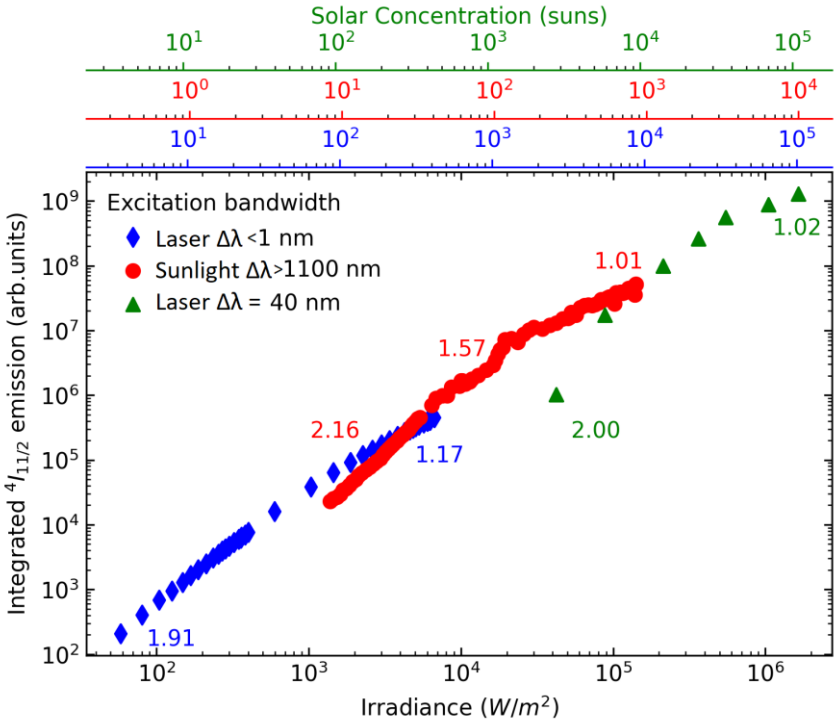

Figure 5: Integrated intensity of the UCPL of the $^4I_{11/2} \rightarrow {}^4I_{15/2}$ transition of β-NaYF$_4$: 25%Er^{3+} under laser and sunlight excitations, with the numbers along the curve indicating the slopes in the low, medium and high intensity regimes.

The measured time-dependent kinetics of the UCPL (**Fig. S4**) indicate that the reduced UCPL is not an effect of increased temperature. To further investigate additional population pathways, we measured the diffuse reflectance spectra of samples with a different Er^{3+} ion content. It can be seen in **Fig. 6** that, in addition to the bands from $^4I_{15/2} \rightarrow {}^4I_{11/2}$ at 980 nm and $^4I_{15/2} \rightarrow {}^4I_{13/2}$ at 1520 nm, there are additional absorption bands. The reflectance at 980 nm and 1520 nm decreases as the Er^{3+} ion content increases, consistent with a higher absorption. The lower reflectance with increased Er^{3+} ion content outside the absorption bands indicates lower scattering in the β-$NaYF_4$ microcrystal by substituting Y^{3+} with Er^{3+} ions.

The β-$NaYF_4$: Er^{3+} samples were embedded in a perfluorocyclobutyl (PFCB) host, necessitating a determination of the absorption of the fluoropolymer in the NIR. In fact, the peaks at 1130 nm with a broader shoulder at 1180 nm are in agreement with the 5th and 3rd vibrational harmonics of C-O and C-H, respectively [58]. The broad shoulder at 1380 nm can be associated with the 4th harmonic of C-O, while the line at 1665 nm agrees with the 2nd harmonic of C-H [58]. The peaks at 2145 nm and 2300 nm are possibly associated with higher harmonics of C-F. The energy of the vibrational harmonic bands cannot be transferred to the upconverter and NIR emission is most likely quenched by C-H vibrations in the host enclosing the upconverter. Non-radiative transfer from Er^{3+} ions to a number of hosting solvents [59], [60] and polymers [61] has been widely reported.

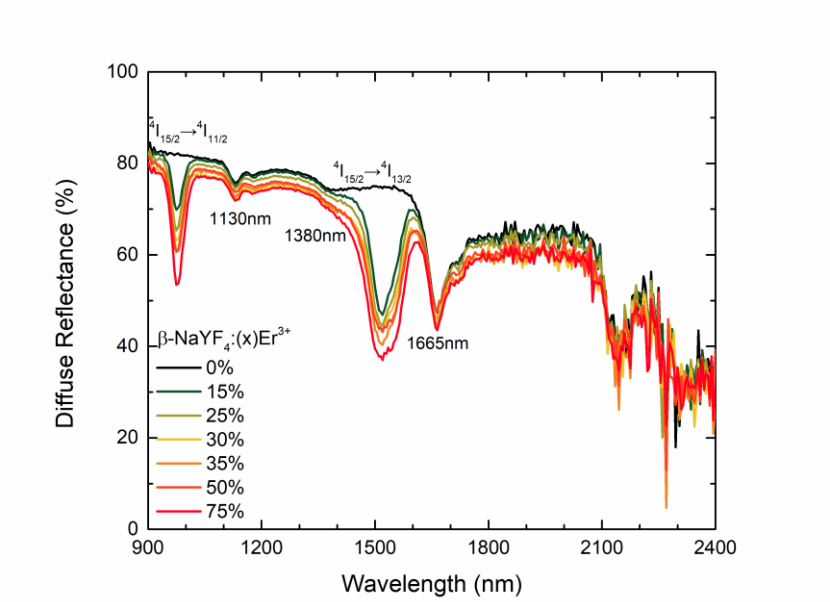

Figure 6: Diffuse reflectance spectra of β-$NaYF_4$: Er^{3+} for varying Er^{3+} ion content.

Higher excited metastable Er^{3+} ion levels may be involved in UC to 980 nm by ESA under sunlight excitation at $\lambda > 1100$ nm. In particular, the transitions $^4I_{13/2} \rightarrow {}^4F_{9/2}$ (1138 nm), $^4I_{11/2} \rightarrow {}^4S_{3/2}$ (1211 nm) and $^4I_{9/2} \rightarrow {}^4F_{7/2}$ (1214 nm). These wavelengths overlap with the spectral absorption of the polymer shown in **Fig. 6**. The absorption from bands outside the Er^{3+} ion GSA should result in lower slopes when exciting the excited states of the Er^{3+} ion [19]. Moreover, when excited by sunlight at wavelengths above 1350 nm, the green, red and NIR upconversion from states $^4S_{3/2}$, $^4F_{9/2}$ and $^4I_{9/2}$, respectively, may indicate the exclusion of the above-mentioned excited state transitions. The emission at 550 and 810 nm was too weak for our setup to provide a meaningful analysis. However, the 660 nm emission under sunlight excitation was intense over a wide range of solar concentration.

To examine the above hypotheses for transitions between 1100 and 1350 nm, we changed the excitation spectrum by filtering the sunlight excitation to $1100 < \lambda$ 1350 nm. We obtained higher

power-dependent slopes at the high solar concentration regime depending on the Er^{3+} ion content, see **Fig. 7**. In addition to β-$NaYF_4$: 25%Er^{3+}, emission at higher and lower concentrations, (i.e. β-$NaYF_4$: 15%Er^{3+} and β-$NaYF_4$: 50%Er^{3+}) were measured to confirm the hypotheses at below-optimal erbium concentrations.

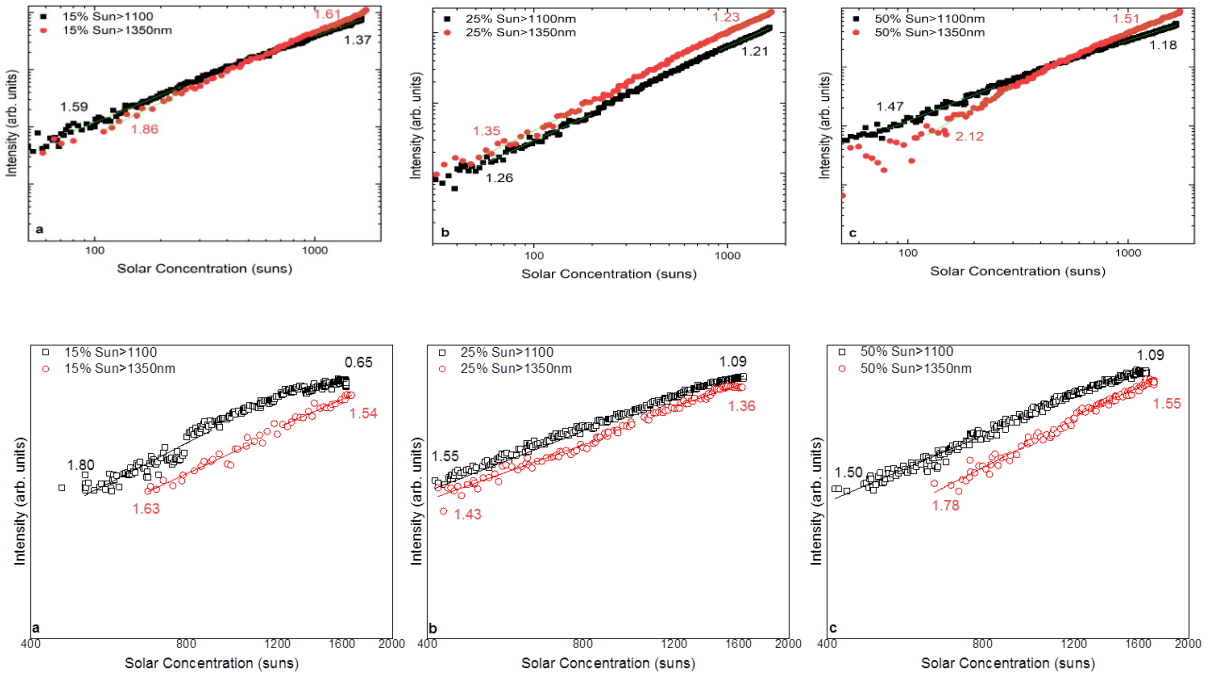

Figure 7: Solar concentration dependence of the 980 nm (solid symbols) and 660 nm (open symbols) UC emission with sunlight excitation at $\lambda > 1100$ nm (squares) and $\lambda > 1350$ nm (circles) for 15%, 25% and 50% Er^{3+} ion content.

The slopes of the 980 nm emission from an excitation at $\lambda > 1350$ nm exceeded those at $\lambda > 1100$ nm excitation for all samples, regardless of erbium concentration. In Fig. 7, the differences in the values of the slopes for the different spectral ranges, between the samples with differing Er^{3+} concentration, can be explained as follows. ETU depends on the Er^{3+} interionic distance, which in turn changes the population between levels and therefore affects the slope when excited by sunlight at λ>1350 nm. In β-$NaYF_4$: Er^{3+}, the average interionic distance for the highest UCQY was reported to vary from 0.6 nm at 30% to 0.7 nm at 20% Er^{3+} ion doping [62]. The distance between Er^{3+} ions is related to its molar content in the host crystal, β-$NaYF_4$, as Er^{3+} substitutes Y^{3+} ions. Therefore, varying the Er^{3+} ion content will directly affect the efficiency of energy transfer and consequently the UCQY. The highest UCQY of β-$NaYF_4$: Er^{3+} was reported at a molar content of 25% and an irradiance of 970 W/m^2 [12], as well as for a molar content of 20% but at the far greater irradiance 1.97×10^6 W/m^2 [20].

The UCQY and the rise times also decrease at a higher molar content [12], but due to concentration quenching. For the sample β-$NaYF_4$: 15%Er^{3+}, the curve saturates when the solar concentration exceeds 1000 suns, indicating an increased red emission when excited with 1100-1350 nm sunlight. The saturation is less pronounced in samples β-$NaYF_4$: 25%Er^{3+} and β-$NaYF_4$: 50%Er^{3+} where a higher molar concentration reduces the probability of ESA in favor of ETU.

The relation between the power-dependent slopes and the molar content was also reported [63] under 1523±10 nm excitation. The curves saturate at a solar concentration of 400-500 suns when a wider absorption band of 1480-1560 nm is used. The saturation limit is based on a semi-empirical relation of the UCQY at an input power density of 10^4 W/m^2 - ascribed to the concentration-dependent depopulation of level $^4I_{11/2}$. A lower threshold was observed with a laser excitation of 20 nm bandwidth.

Under sunlight, however, all Er^{3+} ion levels are resonantly excited [19], so a target solar irradiance lower than that of the laser is required to fully populate level $^4I_{11/2}$ and saturate the two-photon UC. The extrapolated UCQY values under laser [63] and broadband excitation [20] are in reasonable agreement with the UCPL of the samples under the sunlight excitation restricted to $\lambda > 1100$ nm. Upconverters with a low Er^{3+} ion content require higher excitation irradiance and *vice versa*.

Figure 1(a) displays the transitions occurring in β-$NaYF_4$: Er^{3+} are displayed. Sunlight excitation at $\lambda > 1100$ nm is absorbed by the $^4I_{15/2}$ level to the $^4I_{13/2}$ metastable level in the Er^{3+} ion via ground state absorption (GSA) and by the $^4I_{13/2}$ level to the $^4F_{9/2}$ level *via* excited state absorption (ESA), from which emission of 660 nm photons occurs. Energy is transferred to Er^{3+} ions following ETU at the $^4I_{13/2}$ level between two neighbouring Er^{3+} ions. In this process, energy from one ion is transferred to a nearby ion and leads to the $^4I_{9/2}$, $^4F_{9/2}$ *or* $^4F_{7/2}$ levels for the high energy ion, and to the ground state for the low energy ion. Emission of 660 nm and 810 nm photons occurs from levels $^4F_{9/2}$ and $^4I_{9/2}$ respectively. From the $^4I_{9/2}$ and $^4F_{7/2}$ levels, non-radiative relaxation to the $^4S_{3/2}$ and $^4I_{11/2}$ levels is followed by 550 nm and 980 nm emissions, respectively.

Outlook for solar applications

In solar applications, the two-photon UC leading to the emission at $\lambda = 980$ nm will be less efficient above 870±130 suns, due to the population of higher metastable states. This relaxes the requirements for ultra-high concentration optics, and can be realized with existing commercial reflective-refractive concentrators already used for photovoltaic systems [64]. An improvement in the short-circuit current density (ΔJ_{sc}) of 13.3 mA/cm^2 and a relative efficiency increase of 0.19% was reported for β-$NaYF_4$: 25%Er^{3+} in c-Si cells at a cell irradiance of 208 suns [65], While this is about twice the energetically optimum concentration of concentrator c-Si cells, a solar concentration ≥1000 suns is required for upconversion to start being efficient [10]. A higher solar concentration on the upconverter can be further obtained at the back of the solar cell with integrated optics [66], [67], without excluding the requirements for efficient thermal management at high irradiance.

Although a lanthanide upconverter was utilized in this work, efficient solid-state triplet-triplet annihilation (TTA) upconverters have been found for an excitation with visible [68] and sub-1200 nm NIR [69] light. The quest for the later is motivated by its potential to render TTA UC suitable for solar applications such as photocatalysis [70], photochemical water splitting [71] and solar fuels [72] and may be viewed as promising due to the relatively low power densities, sunlight excitation with $\lambda > 500$ nm. Enhanced algal photosynthesis was also reported with spectral shifting, with the onset of saturation and photo-protective reactions at an incoming photon flux density of 70 μmol m^{-2} s^{-1} (of photosynthetically active radiation, which is limited to 400 nm < λ < 700 nm), corresponding to 3-4% of the AM1.5 solar spectrum, and saturation of the photo-productive mechanisms at photon flux density values of 1000-1500 μmol m^{-2} s^{-1}, *i.e.* 50-70% of the AM1.5 irradiance [73]. Numerous upconversion-assisted photocatalysts have been reported in the visible [10] and recently in the NIR [74], [75]. Experiments of NIR photocatalysis have utilized illumination by lasers, NIR lamps or simulated sunlight. Unfortunately, the irradiance of illumination or the solar concentration is rarely reported. Anatase TiO_2 with absorption above 387 nm is commonly utilized as the photocatalyst. The intensity of the solar spectrum at these wavelengths is very low. Therefore the enhancement is achieved by co-doping the TiO_2 photocatalyst to increase its absorption [76] into the NIR by the upconverter. A monotonically higher degradation of methylene blue was demonstrated with a Yb-Er-Tm co-doped ZrF_4–BaF_2–LaF_3–AlF_3–NaF (ZBLAN) upconverter for an irradiance up to 1.5 suns [70]. In photocatalysis experiments with laser illumination, the reported irradiance spanned from 0.50 to 8×10^4 W/m^2 at 980 nm with Yb-Tm [77], [78] and Yb-Er [79] upconverter nanoparticles with a higher energy transfer to a capping layer compared to mixing with the photocatalyst.

Conclusions

We have reported sunlight-excited UC luminescence in β-$NaYF_4$: Er^{3+} with emissions at 980 nm, 810 nm, 660 nm, 550 nm and 525 nm from energy levels $^4I_{11/2}$, $^4I_{9/2}$, $^4F_{9/2}$, $^4S_{3/2}$ and $^2H_{11/2}$, respectively. A power-dependent characterization with concentrated natural sunlight up to 2300 suns was achieved with a double-stage solar furnace. The high solar flux was realized with a reflective-refractive concentrator consisting of a parabolic reflector followed by a truncated pyramidal dielectric light pipe. To ensure the optimal cell efficiency, the silicon solar cell was sited in front of the focus of the primary parabolic reflector, thereby maintaining a solar concentration of 15 suns. In this UC system of β-$NaYF_4$: 25%Er^{3+}, we obtained a two-to-one photon UC threshold of 320 suns under concentrated sunlight limited to $\lambda > 1100$ nm. This infrared sunlight excitation provided additional photons resulting in a lower threshold due to excited state absorption and evidenced by the absence of sunlight over $\lambda = 1100$-1350 nm. The approach presented here demonstrates routes for extending UC luminescence to broader bandwidths that involve pathways in addition to ground state absorption for enhanced solar UC. Our results for the demonstrated two-to-one photon upconversion threshold constitutes a first-ever benchmark for UC with natural concentrated sunlight, in one of the most efficient upconverters to date, β-$NaYF_4$: Er^{3+}. These results point the way to further progress in more efficient upconverters with lower thresholds and provide a direct basis for comparison. Finally, the obtained UC threshold of 320 suns relaxes the requirements of high solar concentration optics, making UC more accessible in solar energy applications most notably photovoltaics, as well as photocatalysis.

Acknowledgements

G.E.A. wishes to thank the Jacob Blaustein Center for Scientific Cooperation for support via a postdoctoral research fellowship, K. Krämer for provision of upconverter materials, as well as G. Moses and V. Melnichak for help with illustrations and experimental configurations.

References

[1] F. Auzel, "Upconversion and anti-stokes processes with f and d ions in solids," *Chem. Rev.*, vol. 104, no. 1, pp. 139–174, Jan. 2004, doi: 10.1021/cr020357g.

[2] A. Fernandez-Bravo *et al.*, "Continuous-wave upconverting nanoparticle microlasers," *Nature Nanotechnology*, vol. 13, no. 7, pp. 572–577, Jul. 2018, doi: 10.1038/s41565-018-0161-8.

[3] B. Zhou, B. Shi, D. Jin, and X. Liu, "Controlling upconversion nanocrystals for emerging applications," *Nat Nano*, vol. 10, no. 11, Art. no. 11, Nov. 2015, doi: 10.1038/nnano.2015.251.

[4] Q. Liu, Y. Zhang, C. S. Peng, T. Yang, L.-M. Joubert, and S. Chu, "Single upconversion nanoparticle imaging at sub-10 W cm−2 irradiance," *Nature Photon*, vol. 12, no. 9, pp. 548–553, Sep. 2018, doi: 10.1038/s41566-018-0217-1.

[5] B. Yoon, J. Lee, I. Sung Park, S. Jeon, J. Lee, and J.-M. Kim, "Recent functional material based approaches to prevent and detect counterfeiting," *Journal of Materials Chemistry C*, vol. 1, no. 13, pp. 2388–2403, 2013, doi: 10.1039/C3TC00818E.

[6] V. Kumar, S. Dottermusch, N. Katumo, A. Chauhan, B. S. Richards, and I. A. Howard, "Unclonable Anti-Counterfeiting Labels Based on Microlens Arrays and Luminescent Microparticles," *Advanced Optical Materials*, vol. 10, no. 9, p. 2102402, 2022, doi: 10.1002/adom.202102402.

[7] G. Gao *et al.*, "Up-Conversion fluorescent labels for plastic recycling: a review," *Adv. Sustainable Syst.*, vol. 1, no. 5, p. 1600033, May 2017, doi: 10.1002/adsu.201600033.

[8] G. E. Arnaoutakis and B. S. Richards, "Geometrical concentration for enhanced up-conversion: A review of recent results in energy and biomedical applications," *Optical Materials*, vol. 83, pp. 47–54, Sep. 2018, doi: 10.1016/j.optmat.2018.05.064.

[9] S. Fischer *et al.*, "Upconversion solar cell measurements under real sunlight," *Optical Materials*, vol. 84, pp. 389–395, Oct. 2018, doi: 10.1016/j.optmat.2018.05.072.

[10] B. S. Richards, D. Hudry, D. Busko, A. Turshatov, and I. A. Howard, "Photon Upconversion for Photovoltaics and Photocatalysis: A Critical Review," *Chem. Rev.*, vol. 121, no. 15, pp. 9165–9195, Aug. 2021, doi: 10.1021/acs.chemrev.1c00034.

[11] T. Trupke, M. A. Green, and P. Würfel, "Improving solar cell efficiencies by up-conversion of sub-band-gap light," *Journal of Applied Physics*, vol. 92, no. 7, pp. 4117–4122, Sep. 2002, doi: 10.1063/1.1505677.

[12] A. Ivaturi *et al.*, "Optimizing infrared to near infrared upconversion quantum yield of β-NaYF4:Er3+ in fluoropolymer matrix for photovoltaic devices," *Journal of Applied Physics*, vol. 114, p. 013505, Jul. 2013, doi: 10.1063/1.4812578.

[13] R. Martín-Rodríguez *et al.*, "Highly efficient IR to NIR upconversion in Gd2O2S: Er3+ for photovoltaic applications," *Chem. Mater.*, vol. 25, no. 9, pp. 1912–1921, May 2013, doi: 10.1021/cm4005745.

[14] S. Fischer, E. Favilla, M. Tonelli, and J. C. Goldschmidt, "Record efficient upconverter solar cell devices with optimized bifacial silicon solar cells and monocrystalline BaY2F8:30% Er3+ upconverter," *Solar Energy Materials and Solar Cells*, vol. 136, pp. 127–134, May 2015, doi: 10.1016/j.solmat.2014.12.023.

[15] J. C. Goldschmidt and S. Fischer, "Upconversion for photovoltaics – a review of materials, devices and concepts for performance enhancement," *Advanced Optical Materials*, vol. 3, no. 4, pp. 510–535, Apr. 2015, doi: 10.1002/adom.201500024.

[16] R. Singh *et al.*, "Harvesting Sub-bandgap Photons via Upconversion for Perovskite Solar Cells," *ACS Appl. Mater. Interfaces*, Nov. 2021, doi: 10.1021/acsami.1c13477.

[17] M. Pollnau, D. R. Gamelin, S. R. Lüthi, H. U. Güdel, and M. P. Hehlen, "Power dependence of upconversion luminescence in lanthanide and transition-metal-ion systems," *Phys. Rev. B*, vol. 61, no. 5, pp. 3337–3346, Feb. 2000, doi: 10.1103/PhysRevB.61.3337.

[18] J. F. Suyver, A. Aebischer, S. García-Revilla, P. Gerner, and H. U. Güdel, "Anomalous power dependence of sensitized upconversion luminescence," *Physical Review B*, vol. 71, no. 12, p. 125123, Mar. 2005, doi: 10.1103/PhysRevB.71.125123.

[19] K. W. Krämer, "Resonance in Er3+ upconversion excitation," *Journal of Luminescence*, vol. 189, no. Supplement C, pp. 78–83, Sep. 2017, doi: 10.1016/j.jlumin.2016.11.056.

[20] S. K. W. MacDougall, A. Ivaturi, J. Marques-Hueso, K. W. Krämer, and B. S. Richards, "Broadband photoluminescent quantum yield optimisation of Er3+-doped β-NaYF4 for upconversion in silicon solar cells," *Solar Energy Materials and Solar Cells*, vol. 128, pp. 18–26, Sep. 2014, doi: 10.1016/j.solmat.2014.05.004.

[21] S. Fischer, B. Fröhlich, H. Steinkemper, K. W. Krämer, and J. C. Goldschmidt, "Absolute upconversion quantum yield of β-NaYF4 doped with Er3+ and external quantum efficiency of upconverter solar cell devices under broad-band excitation considering spectral mismatch corrections," *Solar Energy Materials and Solar Cells*, vol. 122, pp. 197–207, Mar. 2014, doi: 10.1016/j.solmat.2013.12.001.

[22] G. E. Arnaoutakis *et al.*, "Enhanced energy conversion of up-conversion solar cells by the integration of compound parabolic concentrating optics," *Solar Energy Materials and Solar Cells*, vol. 140, pp. 217–223, Sep. 2015, doi: 10.1016/j.solmat.2015.04.020.

[23] C. L. M. Hofmann *et al.*, "Experimental validation of a modeling framework for upconversion enhancement in 1D-photonic crystals," *Nature Communications*, vol. 12, no. 1, Art. no. 1, Jan. 2021, doi: 10.1038/s41467-020-20305-x.

[24] H. Liu *et al.*, "Balancing power density based quantum yield characterization of upconverting nanoparticles for arbitrary excitation intensities," *Nanoscale*, vol. 5, no. 11, pp. 4770–4775, 2013, doi: 10.1039/C3NR00469D.

[25] M. Oldenburg *et al.*, "Photon upconversion at crystalline organic–organic heterojunctions," *Advanced Materials*, vol. 28, no. 38, pp. 8477–8482, 2016, doi: 10.1002/adma.201601718.

[26] F. Meinardi *et al.*, "Quasi-thresholdless photon upconversion in metal–organic framework nanocrystals," *Nano Lett.*, vol. 19, no. 3, pp. 2169–2177, Mar. 2019, doi: 10.1021/acs.nanolett.9b00543.

[27] D. J. Garfield *et al.*, "Enrichment of molecular antenna triplets amplifies upconverting nanoparticle emission," *Nature Photon*, vol. 12, no. 7, pp. 402–407, Jul. 2018, doi: 10.1038/s41566-018-0156-x.

[28] H. N. Luitel, S. Mizuno, T. Tani, and Y. Takeda, "Broadband-sensitive Ni2+–Er3+ based upconverters for crystalline silicon solar cells," *RSC Adv.*, vol. 6, no. 60, pp. 55499–55506, Jun. 2016, doi: 10.1039/C6RA10713C.

[29] A. C. Pan, C. del Cañizo, E. Cánovas, N. M. Santos, J. P. Leitão, and A. Luque, "Enhancement of up-conversion efficiency by combining rare earth-doped phosphors with PbS quantum dots," *Solar Energy Materials and Solar Cells*, vol. 94, no. 11, pp. 1923–1926, Nov. 2010, doi: 10.1016/j.solmat.2010.06.028.

[30] J. Marques-Hueso, R. Peretti, R. Abargues, B. S. Richards, C. Seassal, and J. P. Martínez-Pastor, "Photonic crystal-driven spectral concentration for upconversion photovoltaics," *Advanced Optical Materials*, vol. 3, no. 4, pp. 568–574, Apr. 2015, doi: 10.1002/adom.201400402.

[31] J. Christiansen, H. Lakhotiya, E. Eriksen, S. P. Madsen, P. Balling, and B. Julsgaard, "Analytical model for the intensity dependence of 1500 nm to 980 nm upconversion in Er3+: A new tool for material characterization," *Journal of Applied Physics*, vol. 125, no. 4, p. 043106, Jan. 2019, doi: 10.1063/1.5064409.

[32] R. E. Joseph *et al.*, "Critical Power Density: A Metric To Compare the Excitation Power Density Dependence of Photon Upconversion in Different Inorganic Host Materials," *J. Phys. Chem. A*, vol. 123, pp. 6799–6811, Jul. 2019, doi: 10.1021/acs.jpca.9b03851.

[33] S. K. W. MacDougall, A. Ivaturi, J. Marques-Hueso, K. W. Krämer, and B. S. Richards, "Ultra-high photoluminescent quantum yield of β-$NaYF_4$: 10% Er^{3+} via broadband excitation of upconversion for photovoltaic devices," *Opt. Express, OE*, vol. 20, no. 106, pp. A879–A887, Nov. 2012, doi: 10.1364/OE.20.00A879.

[34] S. K. W. MacDougall, A. Ivaturi, J. Marques-Hueso, and B. S. Richards, "Measurement procedure for absolute broadband infrared up-conversion photoluminescent quantum yields: Correcting for absorption/re-emission," *Review of Scientific Instruments*, vol. 85, no. 6, p. 063109, Jun. 2014, doi: 10.1063/1.4881537.

[35] S. Fischer, R. Martín-Rodríguez, B. Fröhlich, K. W. Krämer, A. Meijerink, and J. C. Goldschmidt, "Upconversion quantum yield of Er3+-doped β-NaYF4 and Gd2O2S: The effects of host lattice, Er3+ doping, and excitation spectrum bandwidth," *Journal of Luminescence*, vol. 153, pp. 281–287, Sep. 2014, doi: 10.1016/j.jlumin.2014.03.047.

[36] M. Lin, S. Cheng, X. Wu, S. Zhan, and Y. Liu, "Optical temperature sensing based on upconversion nanoparticles with enhanced sensitivity via dielectric superlensing modulation," *J Mater Sci*, vol. 56, no. 17, pp. 10438–10448, Jun. 2021, doi: 10.1007/s10853-021-05943-w.

[37] P. Manley *et al.*, "Double-layer metasurface for enhanced photon up-conversion," *APL Photonics*, vol. 6, no. 3, p. 036103, Mar. 2021, doi: 10.1063/5.0040839.

[38] Q. Liu, H. Liu, D. Li, W. Qiao, G. Chen, and H. Ågren, "Microlens array enhanced upconversion luminescence at low excitation irradiance," *Nanoscale*, vol. 11, no. 29, pp. 14070–14078, 2019, doi: 10.1039/C9NR03105G.

[39] L. Liang *et al.*, "Upconversion amplification through dielectric superlensing modulation," *Nat Commun*, vol. 10, no. 1, p. 1391, Mar. 2019, doi: 10.1038/s41467-019-09345-0.

[40] Y. Ji *et al.*, "Huge upconversion luminescence enhancement by a cascade optical field modulation strategy facilitating selective multispectral narrow-band near-infrared photodetection," *Light Sci Appl*, vol. 9, no. 1, p. 184, Oct. 2020, doi: 10.1038/s41377-020-00418-0.

[41] R. Winston and J. M. Gordon, "Planar concentrators near the étendue limit," *Opt. Lett., OL*, vol. 30, no. 19, pp. 2617–2619, Oct. 2005, doi: 10.1364/OL.30.002617.

[42] A. Goldstein and J. M. Gordon, "Tailored solar optics for maximal optical tolerance and concentration," *Solar Energy Materials and Solar Cells*, vol. 95, no. 2, pp. 624–629, Feb. 2011, doi: 10.1016/j.solmat.2010.09.029.

[43] K. W. Krämer, D. Biner, G. Frei, H. U. Güdel, M. P. Hehlen, and S. R. Lüthi, "Hexagonal sodium yttrium fluoride based green and blue emitting upconversion phosphors," *Chemistry of Materials*, vol. 16, no. 7, pp. 1244–1251, Apr. 2004, doi: 10.1021/cm031124o.

[44] J. Kettle *et al.*, "Printable luminescent down shifter for enhancing efficiency and stability of organic photovoltaics," *Solar Energy Materials and Solar Cells*, vol. 144, pp. 481–487, Jan. 2016, doi: 10.1016/j.solmat.2015.09.037.

[45] C. Würth, P. Manley, R. Voigt, D. Ahiboz, C. Becker, and U. Resch-Genger, "Metasurface Enhanced Sensitized Photon Upconversion: Toward Highly Efficient Low Power Upconversion Applications and Nanoscale E-Field Sensors," *Nano Lett.*, vol. 20, no. 9, pp. 6682–6689, Sep. 2020, doi: 10.1021/acs.nanolett.0c02548.

[46] E. A. Katz, J. M. Gordon, W. Tassew, and D. Feuermann, "Photovoltaic characterization of concentrator solar cells by localized irradiation," *Journal of Applied Physics*, vol. 100, no. 4, p. 044514, Aug. 2006, doi: 10.1063/1.2266161.

[47] J. M. Gordon, D. Babai, and D. Feuermann, "A high-irradiance solar furnace for photovoltaic characterization and nanomaterial synthesis," *Solar Energy Materials and Solar Cells*, vol. 95, no. 3, pp. 951–956, Mar. 2011, doi: 10.1016/j.solmat.2010.11.030.

[48] G. E. Arnaoutakis, J. Marques-Hueso, B. S. Richards, and T. K. Mallick, "Propagation of white light through optical fibres for CPV systems," in *SPIE Photonics Europe*, International Society for Optics and Photonics, 2012, pp. 843811–843811. Accessed: Mar. 15, 2016. [Online]. Available: http://proceedings.spiedigitallibrary.org/proceeding.aspx?articleid=1316635

[49] P. S. May and M. Berry, "Tutorial on the acquisition, analysis, and interpretation of upconversion luminescence data," *Methods Appl. Fluoresc.*, vol. 7, no. 2, p. 023001, Feb. 2019, doi: 10.1088/2050-6120/ab02c6.

[50] G. E. Arnaoutakis *et al.*, "Enhanced up-conversion for photovoltaics via concentrating integrated optics," *Opt. Express, OE*, vol. 22, no. 102, pp. A452–A464, Mar. 2014, doi: 10.1364/OE.22.00A452.

[51] R. Fenske and G. Arnaoutakis, "Photoluminescence spectroscopy of rare earth doped materials: Why measure at the quantum limit?," in *Proc. 18th Int. Conf. on Transparent Optical Networks (ICTON)*, IEEE, Jul. 2016. doi: 10.1109/ICTON.2016.7550714.

[52] P. Lutsyk *et al.*, "Self-assembly for two types of J-aggregates: cis-Isomers of dye on the carbon nanotube surface and free aggregates of dye trans-isomers," *J. Phys. Chem. C*, vol. 123, pp. 19903–19911, Jul. 2019, doi: 10.1021/acs.jpcc.9b03341.

[53] R. Guo *et al.*, "Initial stages of photodegradation of MAPbI3 perovskite: accelerated aging with concentrated sunlight," *Solar RRL*, vol. 0, no. 0, p. 1900270, 2019, doi: 10.1002/solr.201900270.

[54] R. E. Joseph *et al.*, "A method for correcting the excitation power density dependence of upconversion emission due to laser-induced heating," *Optical Materials*, vol. 82, pp. 65–70, Aug. 2018, doi: 10.1016/j.optmat.2018.05.025.

[55] J. M. Gordon, G. Moses, and E. A. Katz, "Boosting silicon photovoltaic efficiency from regasification of liquefied natural gas," *Energy*, vol. 214, p. 118907, Jan. 2021, doi: 10.1016/j.energy.2020.118907.

[56] A. Shalav, B. Richards, K. Kramer, G. Conibeer, and M. Green, "Two Colour Excitation Up-Conversion Efficiency Enhancement for a Silicon Photovoltaic Device using Er3+-Doped Phosphors," in *2006 IEEE 4th World Conference on Photovoltaic Energy Conference*, Waikoloa, HI: IEEE, 2006, pp. 45–48. doi: 10.1109/WCPEC.2006.279342.

[57] G. E. Arnaoutakis, J. Marques-Hues, A. Ivaturi, K. W. Krämer, T. K. Mallick, and B. S. Richards, "Enhancement of upconversion for photovoltaics with β-NaYF4:Er3+ and concentrating integrated optics," in *Renewable Energy and the Environment (2013), paper PT3C.4*, Optical Society of America, Nov. 2013, p. PT3C.4. doi: 10.1364/PV.2013.PT3C.4.

[58] J. Ballato, S. H. Foulger, and D. W. Smith, Jr., "Optical properties of perfluorocyclobutyl polymers II Theoretical and experimental attenuation," *J. Opt. Soc. Am. B*, vol. 21, no. 5, pp. 958–967, May 2004, doi: 10.1364/JOSAB.21.000958.

[59] F. T. Rabouw, P. T. Prins, P. Villanueva-Delgado, M. Castelijns, R. G. Geitenbeek, and A. Meijerink, "Quenching Pathways in NaYF4:Er3+,Yb3+ Upconversion Nanocrystals," *ACS Nano*, vol. 12, no. 5, pp. 4812–4823, May 2018, doi: 10.1021/acsnano.8b01545.

[60] B. Huang *et al.*, "Overtone Vibrational Transition-Induced Lanthanide Excited-State Quenching in Yb3+/Er3+-Doped Upconversion Nanocrystals," *ACS Nano*, vol. 12, no. 11, pp. 10572–10575, Nov. 2018, doi: 10.1021/acsnano.8b05095.

[61] M. Bortoluzzi *et al.*, "Preparation of photoluminescent PMMA doped with tris(pyrazol-1-yl)borate lanthanide complexes," *Journal of Luminescence*, vol. 132, no. 9, pp. 2378–2384, Sep. 2012, doi: 10.1016/j.jlumin.2012.04.005.

[62] S. Fischer, B. Fröhlich, K. W. Krämer, and J. C. Goldschmidt, "Relation between excitation power density and Er3+ doping yielding the highest absolute upconversion quantum yield," *J. Phys. Chem. C*, vol. 118, no. 51, pp. 30106–30114, Dec. 2014, doi: 10.1021/jp510209x.

[63] A. Boccolini, J. Marques-Hueso, and B. S. Richards, "Self-absorption in upconverter luminescent layers: impact on quantum yield measurements and on designing optimized photovoltaic devices," *Opt. Lett., OL*, vol. 39, no. 10, pp. 2904–2907, May 2014, doi: 10.1364/OL.39.002904.

[64] H. Mashaal, D. Feuermann, and J. M. Gordon, "Basic categories of dual-contour reflective-refractive aplanats," *Opt. Lett., OL*, vol. 40, no. 21, pp. 4907–4910, Nov. 2015, doi: 10.1364/OL.40.004907.

[65] S. Fischer *et al.*, "Upconverter silicon solar cell devices for efficient utilization of sub-band-gap photons under concentrated solar radiation," *IEEE Journal of Photovoltaics*, vol. 4, no. 1, pp. 183–189, Jan. 2014, doi: 10.1109/JPHOTOV.2013.2282744.

[66] G. E. Arnaoutakis, E. Favilla, M. Tonelli, and B. S. Richards, "Single crystal monolithic upconverter solar cell device tandems with integrated optics," *J. Opt. Soc. Am. B, JOSAB*, vol. 39, no. 1, pp. 239–247, Jan. 2022, doi: 10.1364/JOSAB.437892.

[67] J. Day, S. Senthilarasu, and T. K. Mallick, "Enhanced efficiency for building integrated concentrator photovoltaic modules based on rare earth doped optics," *Solar Energy Materials and Solar Cells*, vol. 199, pp. 83–90, Sep. 2019, doi: 10.1016/j.solmat.2019.04.013.

[68] A. Monguzzi *et al.*, "High efficiency up-converting single phase elastomers for photon managing applications," *Advanced Energy Materials*, vol. 3, no. 5, pp. 680–686, 2013, doi: 10.1002/aenm.201200897.

[69] M. Wu *et al.*, "Solid-state infrared-to-visible upconversion sensitized by colloidal nanocrystals," *Nature Photonics*, vol. 10, no. 1, pp. 31–34, Jan. 2016, doi: 10.1038/nphoton.2015.226.

[70] M. E. Borges, M. Sierra, J. Méndez-Ramos, P. Acosta-Mora, J. C. Ruiz-Morales, and P. Esparza, "Solar degradation of contaminants in water: TiO2 solar photocatalysis assisted by up-conversion luminescent materials," *Solar Energy Materials and Solar Cells*, vol. 155, pp. 194–201, Oct. 2016, doi: 10.1016/j.solmat.2016.06.010.

[71] R. S. Khnayzer, J. Blumhoff, J. A. Harrington, A. Haefele, F. Deng, and F. N. Castellano, "Upconversion-powered photoelectrochemistry," *Chemical Communications*, vol. 48, no. 2, pp. 209–211, 2012, doi: 10.1039/C1CC16015J.

[72] K. Börjesson, D. Dzebo, B. Albinsson, and K. Moth-Poulsen, "Photon upconversion facilitated molecular solar energy storage," *Journal of Materials Chemistry A*, vol. 1, no. 30, pp. 8521–8524, 2013, doi: 10.1039/C3TA12002C.

[73] L. Wondraczek, E. Tyystjärvi, J. Méndez-Ramos, F. A. Müller, and Q. Zhang, "Shifting the sun: solar spectral conversion and extrinsic sensitization in natural and artificial photosynthesis," *Adv. Sci.*, vol. 2, no. 12, p. 1500218, Dec. 2015, doi: 10.1002/advs.201500218.

[74] P. Acosta-Mora *et al.*, "'A bridge over troubled gaps': up-conversion driven photocatalysis for hydrogen generation and pollutant degradation by near-infrared excitation," *Chemical Communications*, vol. 54, no. 15, pp. 1905–1908, 2018, doi: 10.1039/C7CC09774C.

[75] A. A. Ansari and M. Sillanpää, "Advancement in upconversion nanoparticles based NIR-driven photocatalysts," *Renewable and Sustainable Energy Reviews*, vol. 151, p. 111631, Nov. 2021, doi: 10.1016/j.rser.2021.111631.

[76] Z. El Koura *et al.*, "Synthesis and Characterization of Cu and N Codoped RF-Sputtered TiO2 Films: Photoluminescence Dynamics of Charge Carriers Relevant for Water Splitting," *J. Phys. Chem. C*, vol. 120, no. 22, pp. 12042–12050, Jun. 2016, doi: 10.1021/acs.jpcc.6b03058.

[77] Y. Tang, W. Di, X. Zhai, R. Yang, and W. Qin, "NIR-Responsive Photocatalytic Activity and Mechanism of NaYF $_4$:Yb,Tm@TiO $_2$ Core–Shell Nanoparticles," *ACS Catal.*, vol. 3, no. 3, pp. 405–412, Mar. 2013, doi: 10.1021/cs300808r.

[78] M. Tou *et al.*, "Sequential coating upconversion NaYF4:Yb,Tm nanocrystals with SiO2 and ZnO layers for NIR-driven photocatalytic and antibacterial applications," *Materials Science and Engineering: C*, vol. 70, pp. 1141–1148, Jan. 2017, doi: 10.1016/j.msec.2016.03.038.

[79] J. Zhang, Y. Huang, L. Jin, F. Rosei, F. Vetrone, and J. P. Claverie, "Efficient Upconverting Multiferroic Core@Shell Photocatalysts: Visible-to-Near-Infrared Photon Harvesting," *ACS Appl. Mater. Interfaces*, vol. 9, no. 9, pp. 8142–8150, Mar. 2017, doi: 10.1021/acsami.7b00158.

Supplementary material

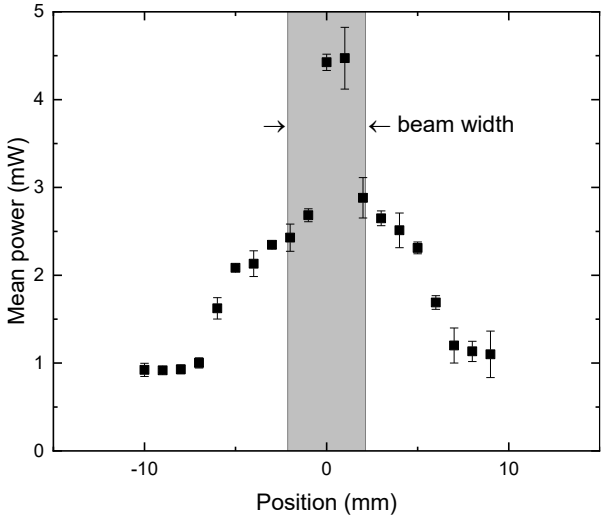

Fig. S1: Intensity profile of the beam of the fibre-optic solar concentrator measured at a distance of 2 mm from the fibre's distal tip with the effective beam width indicated in grey.

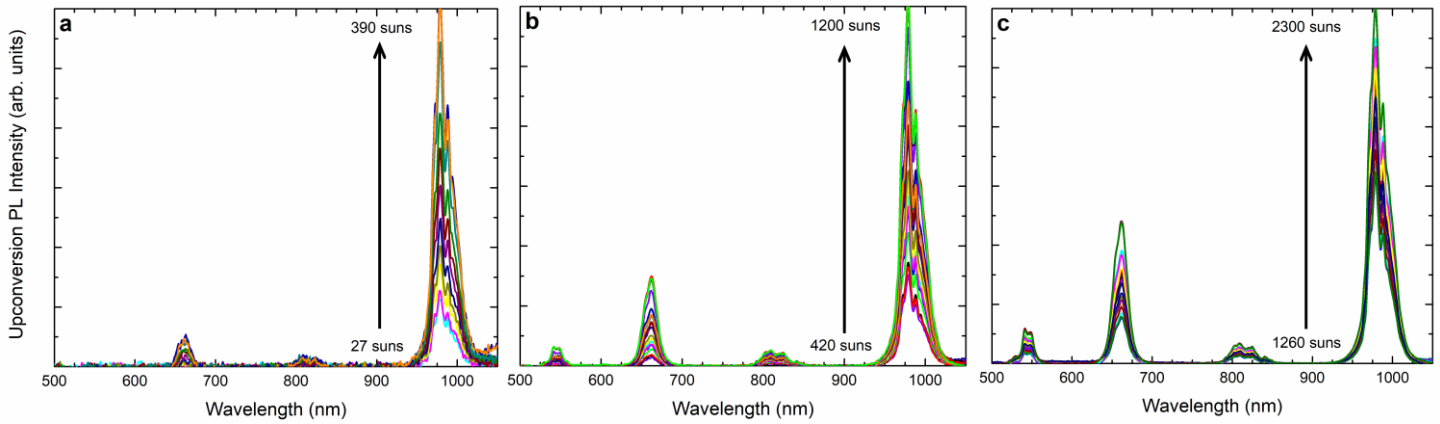

Fig. S2: UC spectra of β-$NaYF_4$: 25%Er^{3+} under solar concentration of a) 27-390 suns, b) 420-1200 suns, c) 1260-2300 suns.

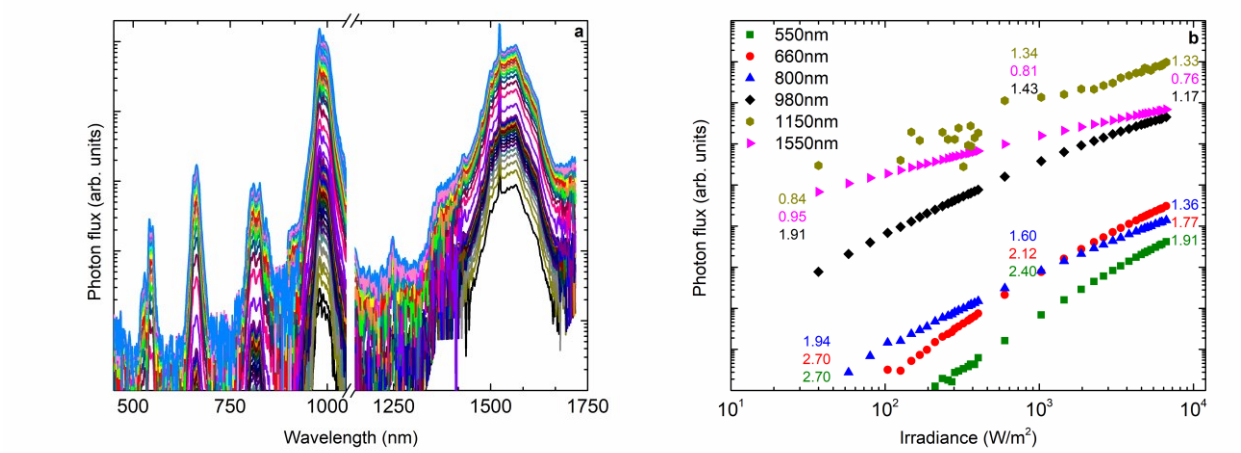

Fig. S3: a) Power-dependent upconversion intensity spectra and b) integrated photon flux of β-$NaYF_4$:25%Er^{3+} at laser irradiance of 37-7000 W/m^2.

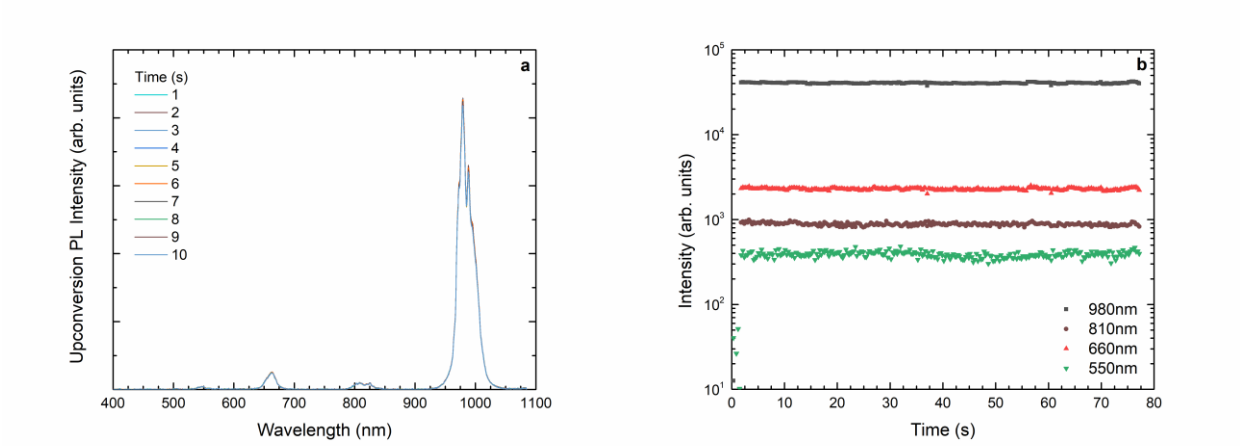

Fig. S4: a) UCPL as a function of time over the initial 10 s of excitation illumination, at a solar concentration of 1680 suns. b) The temporal stability of the intensity of the peaks at 550, 660, 810 and 980 nm over the initial 80 s.